

# The production of proton and lepton fluxes in near Earth orbit

P. Zuccon<sup>1</sup>, B. Bertucci<sup>1</sup>, B. Alpat<sup>1</sup>, R. Battiston<sup>1</sup>, G. Battistoni<sup>2</sup>, W.J. Burger<sup>1</sup>,  
G. Esposito<sup>1</sup>, A. Ferrari<sup>2,3</sup>, E. Fiandrini<sup>1</sup>, G. Lamanna<sup>1,\*</sup>, P.R. Sala<sup>2,3</sup>

January 17, 2002

<sup>1</sup> Università and Sezione INFN of Perugia, Italy

<sup>2</sup> Sezione INFN of Milano, Italy

<sup>3</sup> CERN Switzerland

## Abstract

Substantial fluxes of protons and leptons with energies below the geomagnetic cutoff have been measured by the AMS experiment at altitudes of 370-390 Km, in the latitude interval  $\pm 51.7^\circ$ . The production mechanisms of the observed trapped fluxes are investigated in detail by means of the FLUKA Monte Carlo simulation code. All known processes involved in the interaction of the cosmic protons with the atmosphere (detailed descriptions of the magnetic field and atmospheric density, as well as the electromagnetic and nuclear interaction processes) are included in the simulation. The results are presented and compared with the experimental data, indicating good agreement with the observed fluxes. The impact of secondary proton flux on particle production in atmosphere is briefly discussed.

## 1 Introduction

Cosmic rays approaching the Earth interact with the atmosphere resulting in a substantial flux of secondary particles. The knowledge of composition, intensity and energy spectra of these particles is of considerable interest, e.g. for the evaluation of background radiation for satellites and the estimate of the atmospheric neutrino production for neutrino oscillation experiments [1].

The AMS measurements in near earth orbit [2, 3] have allowed, for the first time, to gather accurate information on the intensity, energy spectra and geographical origin of charged particle fluxes at energies below the geomagnetic cutoff over a wide range of latitudes and at almost all longitudes. The undercutoff component of proton fluxes at equatorial latitudes has revealed an unexpected intensity of up to 50% of the primary proton flux, a positron to electron flux ratio has been found in the undercutoff component which largely exceeds the cosmic one, differences in residence times and geographical origins have been reconstructed for positively and negatively charged particles.

A robust interpretation of these and many other characteristics of the undercutoff fluxes in terms of secondary particles produced in atmosphere requires an accurate description of both the interaction processes at their origin and of the geomagnetic field effects. Recently, different interpretations of

---

\*Now at CERN - Switzerland

the AMS measurements have been proposed [4, 5] based on Monte Carlo simulations using different approaches on both the generation technique and the interaction model.

In this work, we report results from a fully 3D Monte Carlo simulation based on FLUKA 2000 [6] for the description of cosmic ray interactions with the atmosphere. The key features of our analysis are an efficient generation technique for the incoming proton flux and a true microscopic, theory driven treatment of the interaction processes opposite to empirical parametrization of accelerator data. As a first attempt the contribution of  $He$  and the heavier nuclei, representing ( $\approx 9\%$ ) [7] of the all nuclei cosmic flux, is neglected.

In the following section we give a detailed description of the basic ingredients of this simulation, the generation technique and the interaction model. In section 3 we present the results on both protons and leptons and the comparison with AMS measurements. In section 4 we propose our conclusions.

## 2 The model

An isotropic flux of protons is uniformly generated on a geocentric spherical surface with a radius of 1.07 Earth radii ( $\sim 500 Km$  a.s.l.) in the kinetic energy range  $0.1 - 170 GeV$ .

We took the functional form suggested in [8] to describe the proton energy spectrum, the spectral index and the solar modulation parameter are extracted from a fit to the AMS data [9].

The magnetic field in the Earth's proximity includes two components: the Earth's magnetic field, calculated using a 10 harmonics IGRF [10] implementation, and the external magnetic field, calculated using the Tsyganenko Model<sup>1</sup> [11]. To account for the geomagnetic effects, for each primary proton we back-trace an antiproton of the same energy until one of the following conditions is satisfied:

1. the particle reaches the distance of  $10 E_R$  from the Earth's center.
2. the particle touches again the production sphere.
3. neither 1 or 2 is satisfied before a time limit is reached.

If condition 1 is satisfied the particle is on an allowed trajectory, while if condition 2 is satisfied the particle is on a forbidden one. Condition 3 arises for only a small fraction of the events  $O(10^{-6})$ .

Particles on allowed trajectories are propagated forward and can reach the Earth's atmosphere. The atmosphere around the Earth is simulated up to  $120 Km$  a.s.l. using 60 concentric layers of homogeneous density and chemical composition. Data on density and chemical composition are taken from the standard MSIS model [12]. The Earth is modeled as a solid sphere which absorbs each particle reaching its surface.

### 2.1 The generation technique

The ideal approach in the generation of the primary cosmic rays spectra would be to start with an isotropic distribution of particles at a great distance (typically  $10 E_R$ ) from the Earth where the geomagnetic field introduces negligible distortions on the interstellar flux. However, this computational method is intrinsically inefficient since most of the particles are generated with trajectories which will not reach

---

<sup>1</sup>The external magnetic field is calculated only for distances greater than 2 Earth's radii ( $E_R$ ) from the Earth's center. Its contribution to the total magnetic field is  $< 1\%$  at smaller distances and therefore can be safely neglected.

the Earth environment. Kinematic cuts can be applied in order to improve the selection efficiency at generation, however they tend to introduce a bias particles with low rigidity.

A good alternative to this approach is the backtracing method [4],[15] adopted in the present analysis as outlined in the previous section. In the following, we will shortly discuss the validity of the technique and report the results of a comparison of the two methods. We recall that this method was applied for the first time in ref. [8] for the generation of atmospheric neutrino fluxes.

Let us consider first the effects of the geomagnetic field on an incoming flux of charged particles in the absence of a solid Earth. For the discussion, we start with an isotropic flux of monoenergetic<sup>2</sup> protons at large distance, i.e. at infinity, from the origin of a geocentric reference system. In this scenario, a negligible fraction of particles, with very particular initial kinematic parameters, will follow complicated paths and remains confined at a given distance from the origin (semi-bounded trajectories); for all practical purposes this sample can be ignored. Most of the particles will follow unbounded trajectories, reaching again infinity after being deflected by the magnetic field.

Unbounded trajectories cross a spherical surface centered in the field source only an even number of times, as shown in Fig.1: we call *legs* the trajectory parts connecting the spherical surface to infinity and *loops* the parts of the trajectory starting and ending inside the spherical surface.

Since each trajectory can be followed in both directions and no source or sink of particles is contained within the surface, the incoming and outgoing fluxes are the same. However, the presence of the magnetic field breaks the isotropy of the flux “near” the field source, so for a given location there is a flux dependence due to the direction.

Applying the Liouville Theorem, under the hypothesis of isotropy at infinity, it is straightforward to prove [18] that the proton flux in a random point is the same as at infinity along a set of directions (allowed directions), and zero along all the others (forbidden directions).

The pattern of the allowed and forbidden directions depends on both the rigidity and the location and is known as the geomagnetic cutoff.

With the introduction of a solid Earth, all the trajectories that are crossing the Earth are broken in two or more pieces (Fig.2): the *legs* become one-way trajectories and the *loops* disappear.

The presence of the Earth modifies the flux which exits from the surrounding spherical surface, since particles are absorbed by the Earth, while it has only a minimal effect on the incoming flux which is modified only by the absence of certain *loops*. To generate the flux of particles reaching the Earth’s atmosphere, it is sufficient to follow the particles along the allowed trajectories corresponding to the *legs*, taking care to avoid double or multiple counting.

To respect this prescription we reject all trajectories that are back-traced to the production sphere, this allow us to correctly consider the cases like the one shown in Fig.3.

We point out that an important difference with respect to the application in the neutrino flux calculation of [8] is that for the former, the generation sphere coincided with the Earth’s surface, and therefore the forbidden trajectories included those which touched again the Earth (plus those who remained trapped for a long time). In that case there are no problems of double counting.

To check the validity of our technique we made a test comparing the results of the inefficient generation technique at 10 Earth’s radii distance from the Earth’s center with the backtracing technique described in this paper.

---

<sup>2</sup>The realistic case of an energy spectrum can be treated just as a superposition of monenergetic cases

Particle	5GeV		10GeV		20GeV		30GeV	
	Mult.	E frac.	Mult.	E frac.	Mult.	E frac.	Mult.	E frac.
$p$	1.983	0.409	2.676	0.337	2.744	0.307	2.770	0.294
$\pi^+$	0.711	0.131	1.292	0.149	1.970	0.159	2.381	0.164
$\pi^-$	0.389	0.068	0.975	0.098	1.641	0.116	2.047	0.122
$\pi^0$	0.638	0.114	1.601	0.169	2.378	0.175	2.840	0.177

Table 1: Energy fraction and multiplicity of secondary particles for the proton interactions with atmospheric nuclei in FLUKA 2000. Four typical energies of primary protons are considered.

Fig. 4 shows this comparison for several characteristic distributions, the agreement between the two methods is good.

## 2.2 The interaction model

We use the software package FLUKA 2000 [6] to transport the particles and describe their interactions with Earth’s atmosphere. The setup of this simulation is derived from the one used in [1]. This package contains a tridimensional description of both electro-magnetic and hadronic interactions. This code is benchmarked against a wide set of data and is already used in many applications, ranging from low energy nuclear physics to high energy accelerator and cosmic ray physics. For this reason we have preferred this model with respect to the use of “ad hoc” parametrizations of particle production in the energy range of our interest.

In FLUKA hadronic interactions are treated in a theory-driven approach, and the models and their implementations are guided and checked using experimental data. Hadron-nucleon interaction models are based on resonance production and decay below an energy of few  $GeV$  and on the Dual Parton Model above. The extension from hadron to hadron-nucleus interactions is done in the framework of a generalized intra-nuclear cascade approach including the Gribov-Glauber multi-collision mechanism for higher energies followed by equilibrium processes: evaporation, fission, Fermi break-up and  $\gamma$  de-excitation. The parameters of the models embedded in the FLUKA package are fixed only by comparing expectations with data from accelerator experiments.

In fig 5 a) we show the map of the primary proton interaction points in geographical coordinates. The distribution reflects the influence of the geomagnetic cutoff. Fig 5 b) shows the interactions altitude profile, the solid histogram is for  $E_k < 30 GeV$  while the dashed one is for  $E_k > 30 GeV$ . The mean interaction altitude depends weakly on the energy.

The cosmic proton impinging in the atmosphere are doing elastic scattering in the 24% of the events and inelastic interactions in the remaining 76%, in tab.1 we show some characteristic of the inelastic interactions as simulated by FLUKA 2000.

## 3 Comparison with the AMS data

To compare with the AMS data, we define a detection boundary corresponding to a spherical surface at the AMS orbit altitude (400 Km a.s.l). We record each particle that crosses the detection boundary

within the AMS field-of-view, defined as a cone with a  $32^\circ$  aperture with respect to the local zenith or nadir directions.

To obtain the absolute normalization, we take into account the field-of-view, the corresponding AMS acceptance, and an Equivalent Time Exposure (E.T.E.) corresponding to the number of the generated primary protons.

Our results are based on a sample of  $\sim 6 \cdot 10^6$  primary protons generated in the kinetic energy range of  $0.1 - 170 \text{ GeV}$ , which corresponds to  $\sim 4 \cdot 10^{-12} \text{ s}$  (E.T.E.).

### 3.1 Protons

In Fig.6, we show the comparison between the fluxes obtained with the simulation and the measured AMS downgoing proton flux [2] in nine bins of geomagnetic latitude ( $\theta_M$ ) [13]. Fig.7 shows the same comparison for the upgoing proton flux in four selected bins of  $\theta_M$ .

As seen in Fig.6, the simulation well reproduces at all latitudes the high energy part of the spectrum and the falloff in the primary spectrum due to the geomagnetic cutoff, thus validating the general approach used for the generation and detection, as well as the tracing technique.

A good agreement among data and simulation is also found in the under-cutoff part of the spectra. The small and systematic deficit which can be seen in the secondary component of the simulated fluxes is of the same order of the expected contribution from the interaction of cosmic He and heavier nuclei.

This flux is due to the secondaries produced in the atmosphere and that spiral along the geomagnetic field lines up to the detection altitude. Therefore it is sensitive to specific aspects of the interaction model and to the accuracy of the particle transport algorithm.

A correct quantitative prediction of this part of the spectra depends on the quality of low energy nucleon production both in terms of yield and energy distribution. This is in part due to the fragmentation of the target nucleus, and depends on the details of the nuclear physics algorithms describing excitation and break up.

From the analysis of the motion of the secondary protons from their production up to their detection, it can be pointed out that a fraction of the observed flux is due to a multiple counting of the same particles. Within the formalism of adiabatic invariants [16], it is seen that charged particles trapped in the geomagnetic field, i.e. the undercutoff protons, move along drift shells which can be associated with a characteristic residence time<sup>3</sup> that depends on the fraction of the shell located inside the Earth's atmosphere. Thus, particles moving along *long-lived* shells have a large probability to cross many times a geocentered spherical detector, while those moving along *short-lived* shells typically cross the detector only once.

The drift shells crossing the AMS orbit, at an altitude of 400 km, are in general *short-lived*, however in the equatorial region the *long-lived* shells are present as well [17].

In the following, we will indicate as the *real* proton flux that one obtained by counting only once each particle crossing the detector: its intensity is indicated by the dashed distributions in figs. 6 and 7.

A quite relevant effect can be seen in the equatorial region: there the AMS measurement indicates an important secondary proton flux while the *real* number of protons crossing the detector is more than one order of magnitude lower. At high geomagnetic latitudes, the solid and dashed lines tend to merge. The effect becomes negligible for  $\theta_M > 0.8$ .

---

<sup>3</sup>The mean time after which a particle is absorbed into the atmosphere. In our case it represents the effective life time of the particle.

This can be better seen in Fig.8, where the integral primary proton flux seen by AMS is shown as a function of geomagnetic latitude. The intensities of the *real* and measured undercutoff fluxes are reported in the same plot for comparison and their ratio with the primary component shown in Fig.9. A minor contribution from the undercutoff proton component can be therefore expected in the atmospheric shower development and neutrino production.

In Fig.10, the residence time is plotted versus the kinetic energy of the trapped secondary protons for  $|\theta_M| < 0.4$ . In the scatter plot it is possible to distinguish the populations corresponding to *long-lived* and *short-lived* shells similar to those shown in [3] for leptons.

Fig.11 shows the distribution of trapped secondary proton end points for  $|\theta_M| < 0.4$ , Fig.11a is for a lifetimes smaller than 0.3 s., while Fig.11b is for a lifetimes greater than 0.3 s.. The end point distribution agrees with the location of the intersections of the drift shells with the atmosphere as experimentally verified by [2], and discussed in [17].

### 3.2 Electrons and positrons

In Fig. 12 we show a comparison of the simulated undercutoff electron and positron downgoing fluxes with the corresponding AMS measured fluxes [3].

We remind that the AMS positron measurement is restricted at energies below few GeVs, with a dependence of the maximum energy on the geomagnetic latitude which reflects the increasing proton background with  $\theta_m$ .

A comparison of data and simulation in the high energy part of the electron spectra is not possible, since the cosmic electrons have not been used as an input in the current work. However, their contribution to the cosmic rays reaching the atmosphere is  $O(10^{-2})$  leading to a negligible effect of in the generation of the undercutoff fluxes.

The simulation well reproduces the general behavior of the undercutoff part of the spectra in terms of shape and intensity; a similar agreement is observed for the upgoing lepton spectra (not shown). The *real* lepton fluxes, corresponding to the *real* proton flux described earlier, are shown with the dashed line distribution in Fig. 12. As in the case of protons, a large effect from multiple crossing is present going toward the equatorial region, more pronounced for the positron component.

As for the undercutoff protons, we would have expected a systematic deficit in the simulated electron fluxes coming from the missing contribution of helium and heavier nuclei to the CR fluxes. Subcutoff  $e^\pm$  are mainly (97%) coming from decays of pions produced in the proton collisions with the atmospheric nuclei: charged pions contribute through the  $\pi - \mu - e$  chain, while  $\pi^0$  through  $\pi^0 \rightarrow \gamma \gamma$  with subsequent e.m. showers. The relative contribution of charged pions to the subcutoff electrons (positron) fluxes at AMS altitude in our simulation is found to be 37% (47%), while the remaining 60% (50%) appears to come from  $\pi^0$  production. This point deserves some considerations. The level of agreement in the comparison of data and predictions for  $e^\pm$  fluxes turns out to be an important benchmark for the interaction model in view of a discussion on particle production in atmosphere, since is strictly linked to the meson production (mostly pions at this energy). This work complements other studies oriented to the validation of the FLUKA model in terms of particle yields. In particular, the quality of  $\pi^\pm$  generation in our interaction model has been already checked in [19] through the comparison with muon fluxes measurements at different depths in atmosphere. The muons are from the charged pions decay chain and experimental data [20] are well reproduced by the simulation. In the case of  $e^\pm$  also  $\pi^0$ 's become relevant. Usually, when parametrized interaction models are used, like in the works of ref. [4, 14], the

yield of  $\pi^0$  is fixed assuming *a priori* an exact charge symmetry in pion production. In practice, this is also made necessary by the large errors that affect the scarce existing experimental data on neutral pion production. Instead, in the case of a microscopic interaction model like FLUKA, there is no constraint of this type, and the balance of  $\pi^0$  vs.  $\pi^\pm$  automatically emerges from the feature of the model. Recently, it has been pointed out how in FLUKA there exists a significant violation of charge symmetry[21]:  $\pi^0$ 's are in general more ( $\sim 20\%$ ) of the average of  $\pi^+$  and  $\pi^-$ . Technically this symmetry violation emerges in the hadronization of color strings and this normally occurs also in other codes, like JETSET or PITHYA[22]. We cannot enter here in a detailed discussion of this point, and we limit ourselves to say that there are reasons to believe that, at least for laboratory energies below 100 GeV, the acceptable value of charge asymmetry should be lower than that resulting from the present version of the code. However, the comparisons of predictions to data discussed in this work, combined with the mentioned work on atmospheric muons[19], already tell that the predicted fraction of  $\pi^0$  cannot be significantly wrong, although no definitive quantitative conclusion can be extracted, since the nuclear component has not been yet introduced in the primary spectrum.

In Fig.13b-c we show the integrated positron and electron downgoing fluxes for the kinetic energy range  $0.2 - 1.5$  GeV as a function of  $\theta_M$ . Their ratio is shown in Fig.13a. One of the most remarkable features of the AMS measurement is the large value of this ratio, when compared to the natural cosmic value, and its latitude dependence. In Fig. 12, the contribution from primary protons with  $E_k > 30$  GeV to the electron and positron fluxes is illustrated by the filled area. We can notice that in the equatorial region, the electrons are produced essentially by primary protons with  $E_k > 30$  GeV, while for the positrons lower energy protons contribute as well. This distinction disappears at higher latitudes, where positron and electrons are produced by the protons in the same energy range.

This behavior reflects the East-West asymmetry of the geomagnetic cutoff on primary protons and the larger probabilities of escape from atmosphere for secondary electrons(positrons) generated by Westward(Eastward) moving protons [15, 14].

Positrons are preferentially injected on drift shells reaching the AMS altitude by eastward moving protons, which experience a lower rigidity cutoff than westward moving ones. This mechanism is more effective at the equator, where the cutoff is larger and its asymmetry maximal, resulting in the excess of undercutoff positrons from low energy protons as indicated by our simulation. The cutoff mechanism becomes irrelevant at high latitudes, where any difference in positron and electron production should be given instead by different  $\pi^+/\pi^-$  production. Nor the data neither our simulation indicate, within their uncertainties, a relevant charge asymmetry from this source.

## 4 Conclusions

The interactions of cosmic ray protons with the Earth's atmosphere have been investigated by means of a fully 3D Monte Carlo program.

The proton, electron and positron undercutoff flux intensities measured by AMS, as well as their energy spectra, have been correctly reproduced by our simulation

Geomagnetic effects, and in particular the east-west asymmetry in the cosmic protons rigidity cutoff, have been confirmed as the mechanism responsible for the measured excess of the positron component.

The main features of the geographical origin and residence time distributions for both protons and leptons have been replicated and the effect of multiple crossing of the detector by spiraling secondaries

in the geomagnetic field briefly discussed.

Our results indicate that the intensity of the undercutoff proton flux, when the multiple counting is taken into account, never exceeds a 10% of the cosmic proton flux, representing a negligible source for atmospheric production of secondaries. However, this aspect will be object of further and more refined study in the future.

The analysis on the possible strategies to generate the cosmic rays incoming flux has shown the validity of a backtracing approach as an accurate and highly efficient technique.

This work provides also additional way to validate the features of the adopted particle production model. In particular, the study of  $e^\pm$  fluxes has revealed to be to be an interesting instrument to check the meson production in primary interactions, and the results are satisfactory. We believe that our simulation, validated by the high statistic measurements of AMS, can be used to assess the radiation environment in near Earth orbit, and represents a valuable tool for a more accurate calculation of particle fluxes in atmosphere.

*This work has been partially supported by the Italian Space Agency (ASI) under contract ARS-98/47.*



## References

- [1] G. Battistoni et al., *Astropart. Phys.* 12 (2000) 315;
- [2] J.Alcaraz et al., AMS Collaboration, *Phys. Lett. B*472 (2000) 215;
- [3] J.Alcaraz et al., AMS Collaboration, *Phys.Lett. B*484 (2000) 10;
- [4] L. Derome, et al. *Phys. Lett. B*489 (2000) 1;
- [5] V.Plyaskin, *Phys.Lett. B*516 (2001) 213;
- [6] A. Ferrari et al., *Physica Medica*, VOL XVII, Suppl. 1.
- [7] T.K. Gaisser, M. Honda, P. Lipari and T. Stanev, *Proc. of the 27th ICRC (Hamburg, 2001)*, Session OG1.01
- [8] M. Honda et al., *Phys. Rev. D*52 (1995) 4985;
- [9] J.Alcaraz et al., AMS Collaboration, *Phys. Lett. B*490 (2000) 27;
- [10] N.A. Tsyganenko *Geomagn. and Aeronomy* V.26 (1986) 523; N.A. Tsyganenko and M.Peredo, *Geopack Manual*, (1992)
- [11] N.A. Tsyganenko and D.P. Stern, *ISTP newsletter*, 6 (1996) 21;
- [12] A. E. Hedin, *J. Geophys. Res.* 96 (1991) 1151;
- [13] G.Gustaffson et al., *J.Atmos. Terr.Phys* 54 (1992) 1609;
- [14] L.Derome et al., *astro-ph/0103474*;
- [15] P.Lipari, *astro-ph/0101559*;
- [16] C.E.Mc Ilwain, *J. Geophys. Res.* 66(1961) 3681;
- [17] E. Fiandrini et al. *astro-ph/0106241*, E.Fiandrini et al, *Proceedings of the XXVII ICRC (Hamburg)*.
- [18] M.S.Vallarta, *Handbuch der Physik*, Springer, Vol. XLVI/1 (1961) 88;
- [19] G.Battistoni et al., *hep-ph/0107241*;
- [20] M.Boezio et al., *Phys. Rev. D*62 (2000) 032007;
- [21] P. Lipari, *Proc. of the IX Workshop on Neutrino Telescopes, Venice, 2001*.
- [22] T.Sjostrand, *Comp. Phys. Comm.* 82 (1994) 74

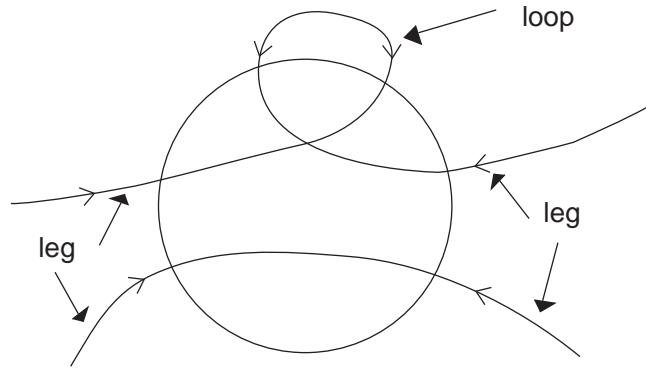


Figure 1: Trajectories types crossing a spherical surface around the Earth

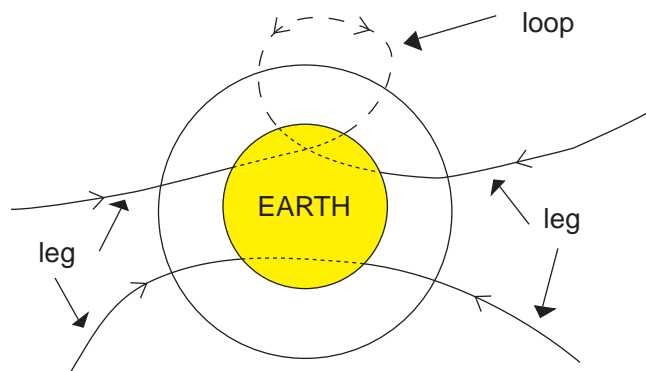


Figure 2: Trajectories in the presence of a solid Earth

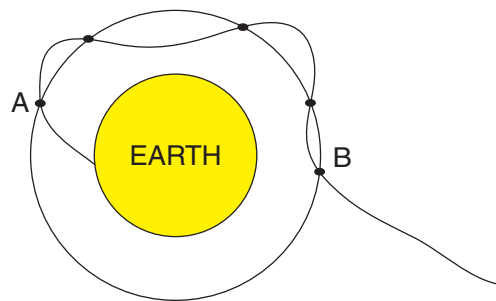


Figure 3: An example of multiple counting along a trajectory, this type of trajectory has to be considered only at point B.

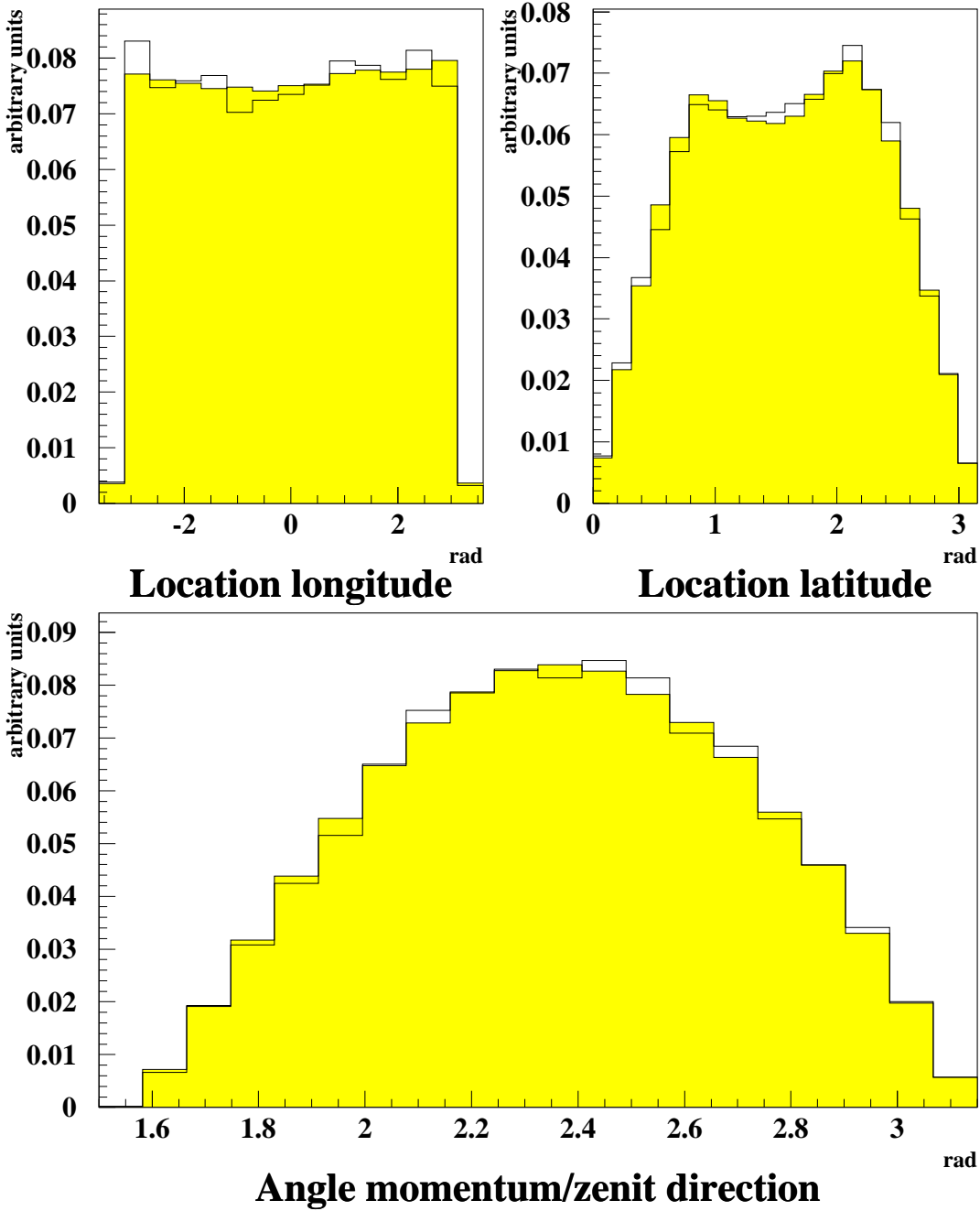


Figure 4: Latitude and longitude of impact points and angle between momentum and zenith directions for particles generated at a distance of 10 Earth's radii (solid line) and particles generated at 1.07 Earth's radii (shaded histogram).

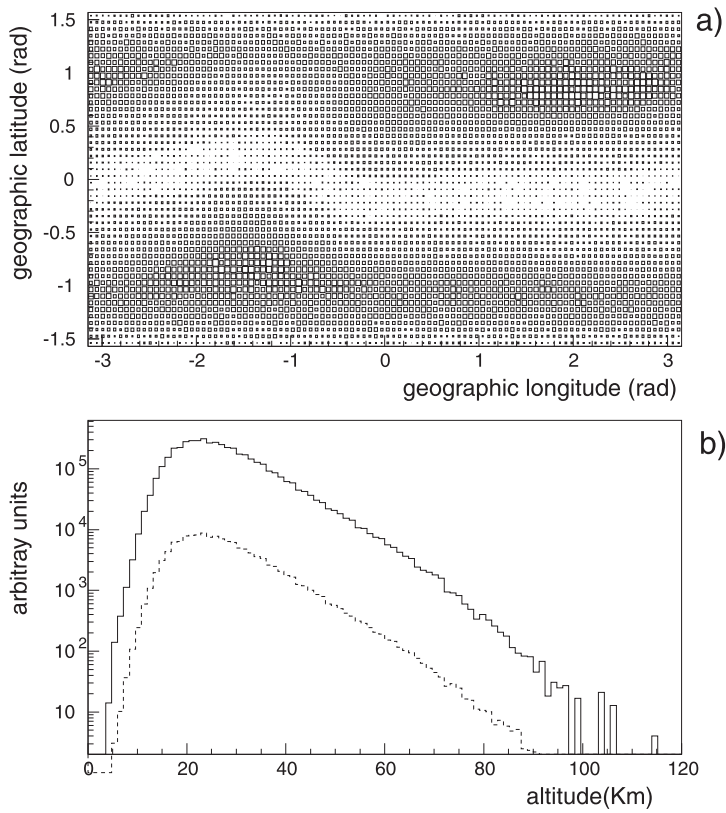


Figure 5: a) distribution of primary protons interaction points in geographical coordinates, b) altitude profile of primary protons interaction points, solid line  $E_k < 30 \text{ GeV}$ , dashed line  $E_k > 30 \text{ GeV}$

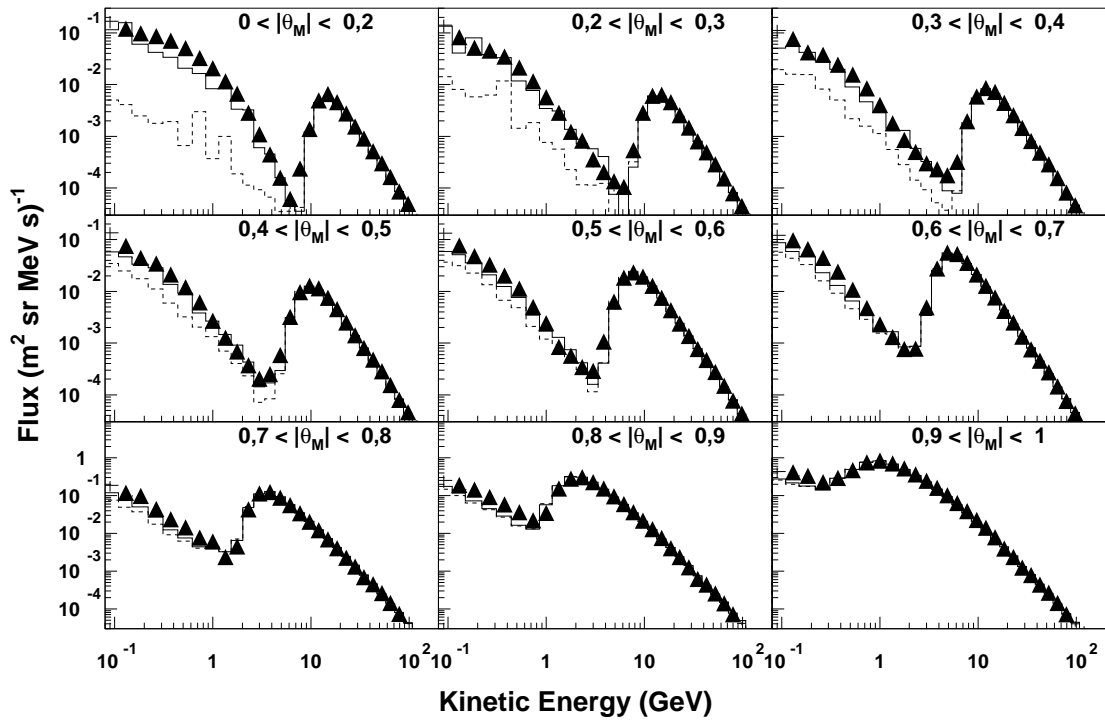


Figure 6: Downgoing proton flux, simulation(solid line) and the AMS data (triangles); the dashed lines are described in the text.  $\Theta_M$  is the geomagnetic latitude in radians.

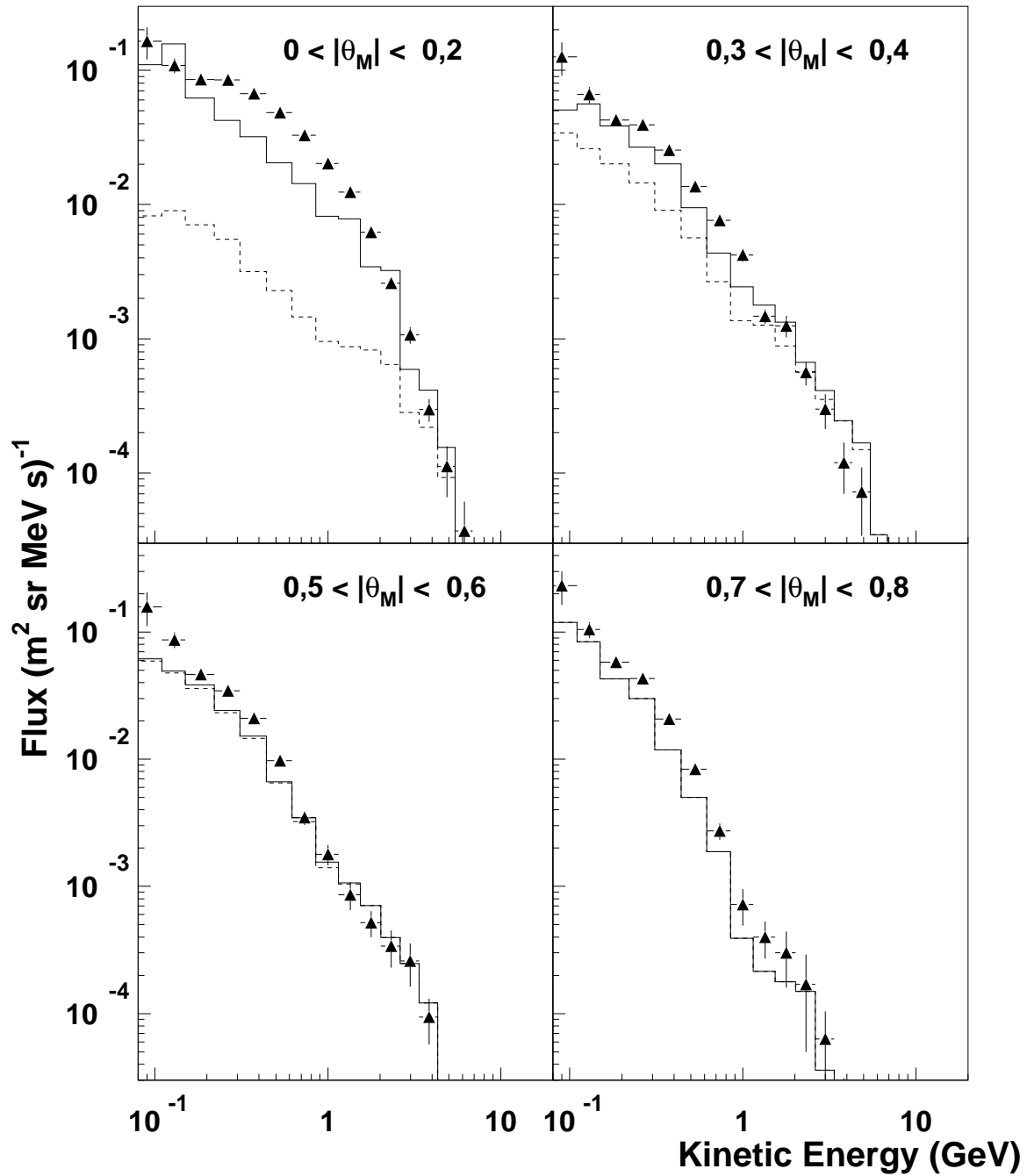


Figure 7: Upgoing proton fluxes, simulation (solid line) and the AMS data (triangles); the dashed lines are described in the text.

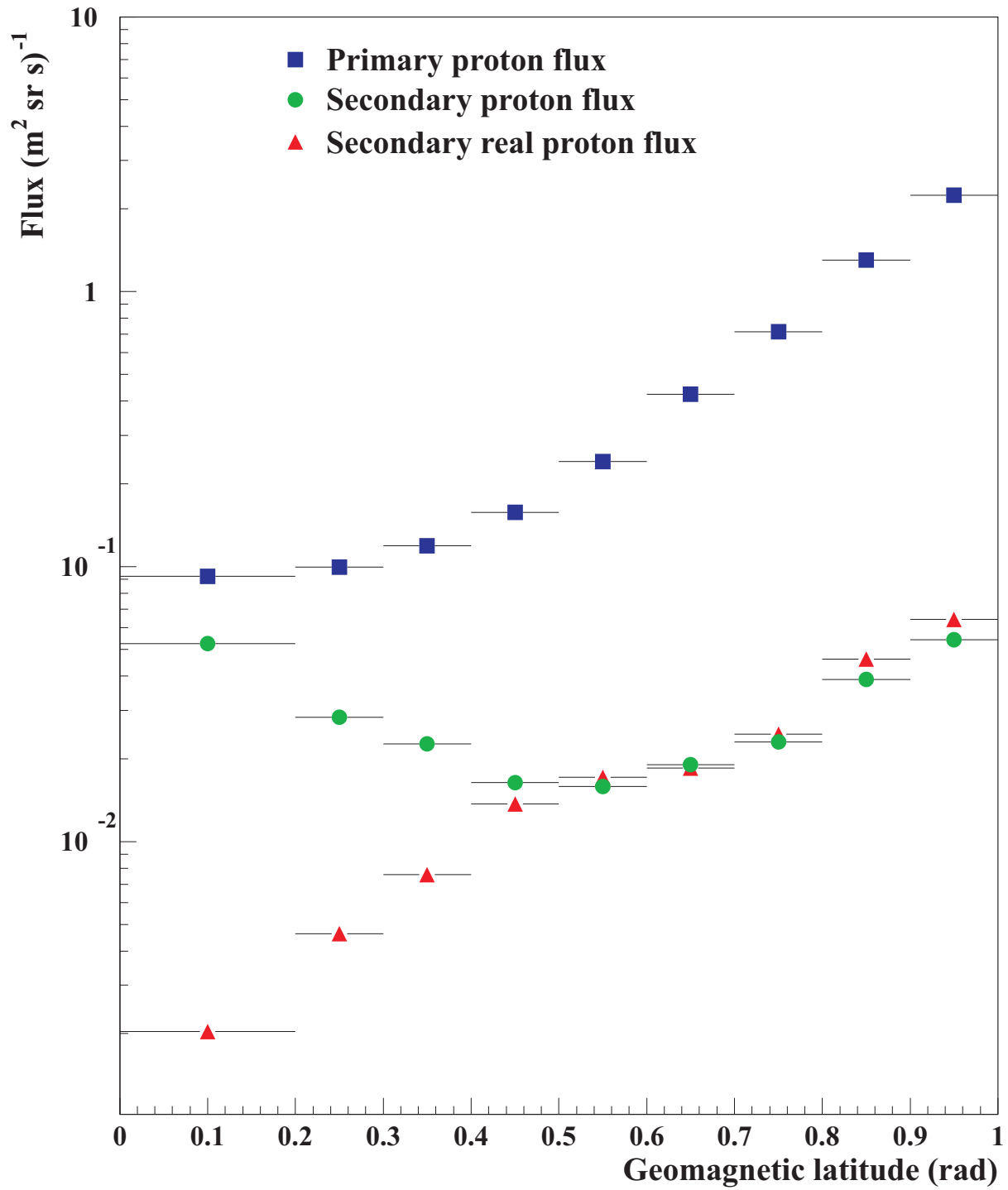


Figure 8: Proton fluxes in the AMS field of view as calculated with this simulation. The fluxes are integrated over the kinetic energy range  $0.1 - 170 \text{ GeV}$  and shown as a function of the geomagnetic latitude.

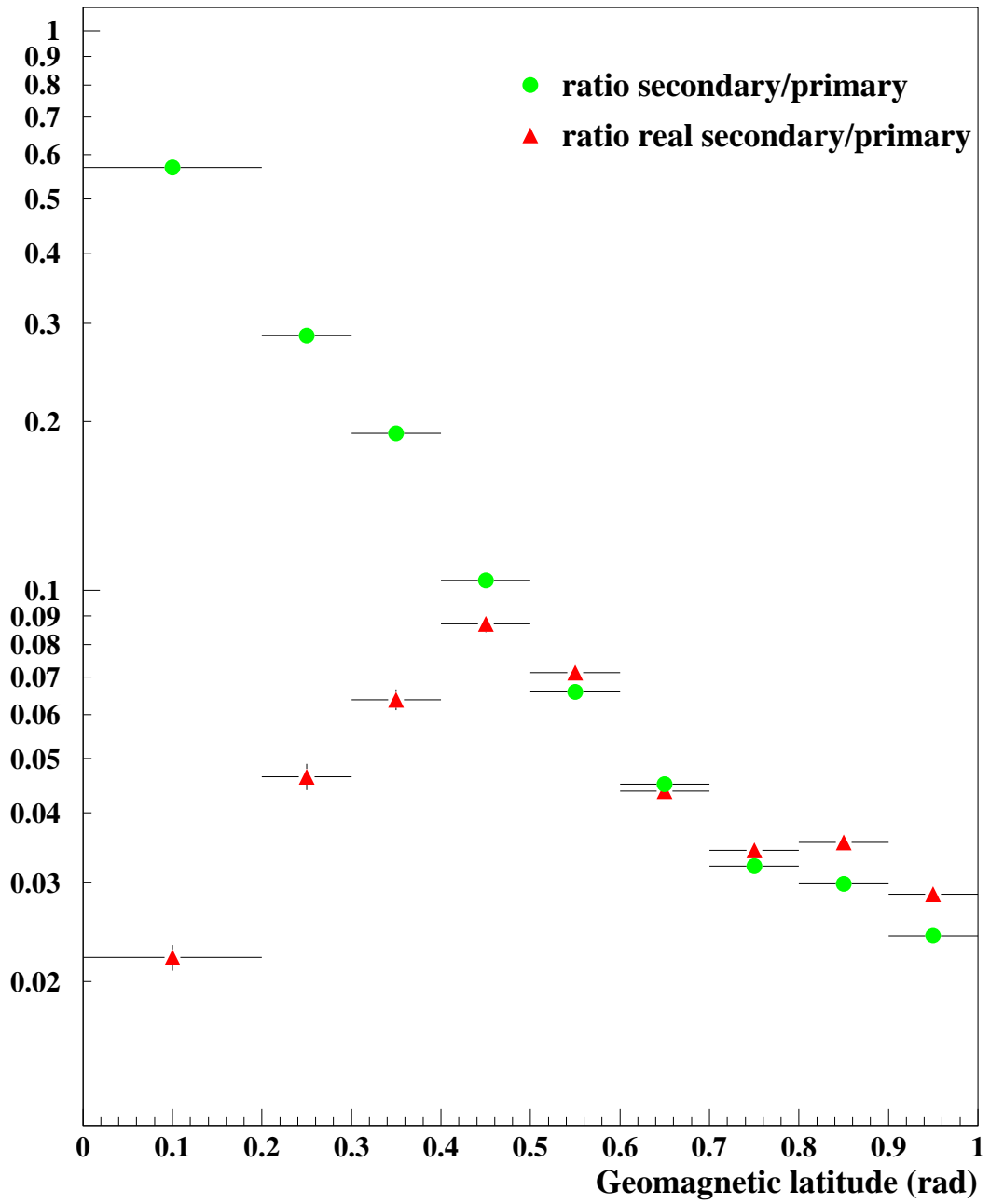


Figure 9: Ratios of the fluxes shown in Fig.8



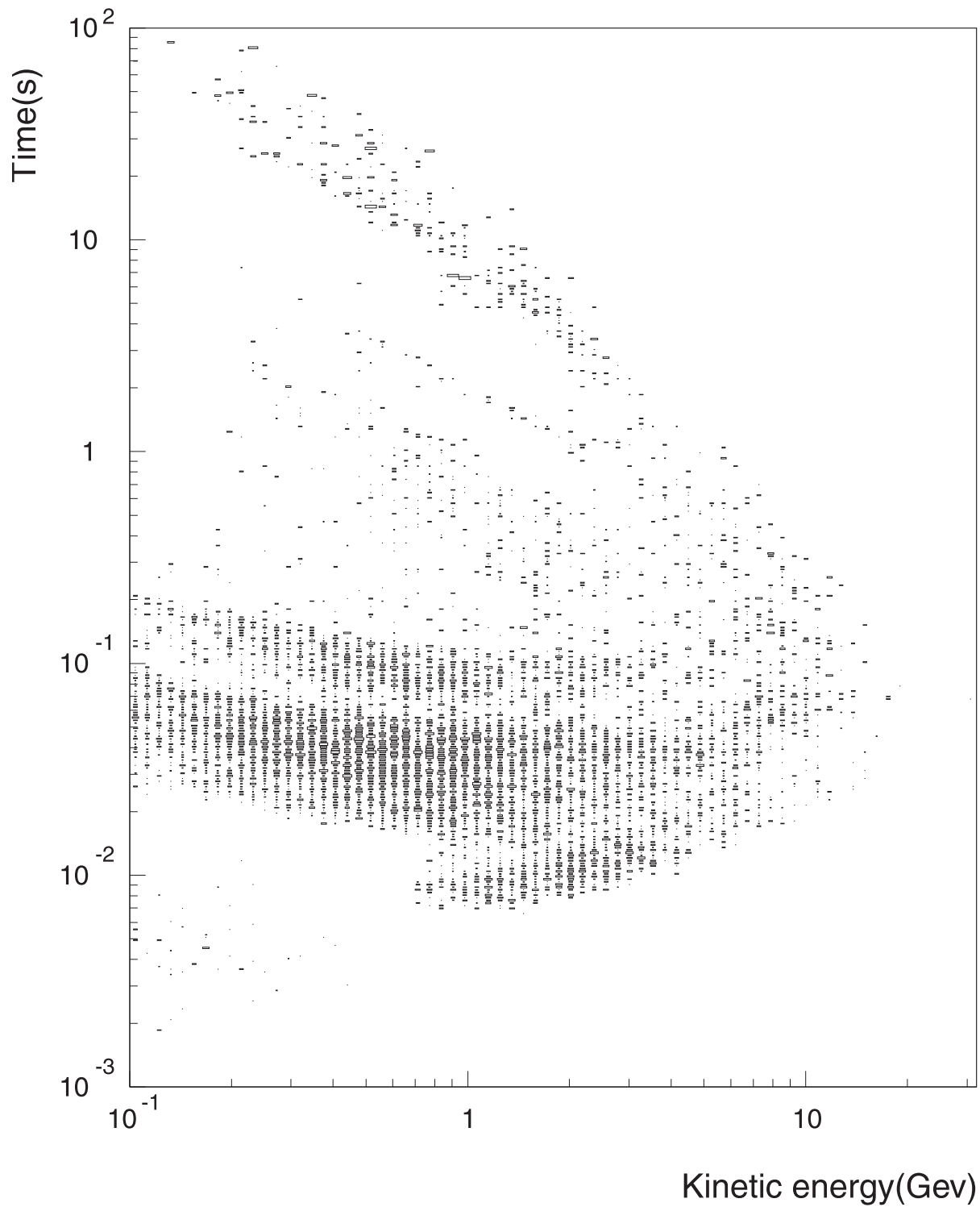


Figure 10: Life time versus kinetic energy for secondary protons produced in the interactions of primary cosmic rays with the atmosphere. The protons are detected at geomagnetic latitude  $|\theta_M| < 0.4$  rad.

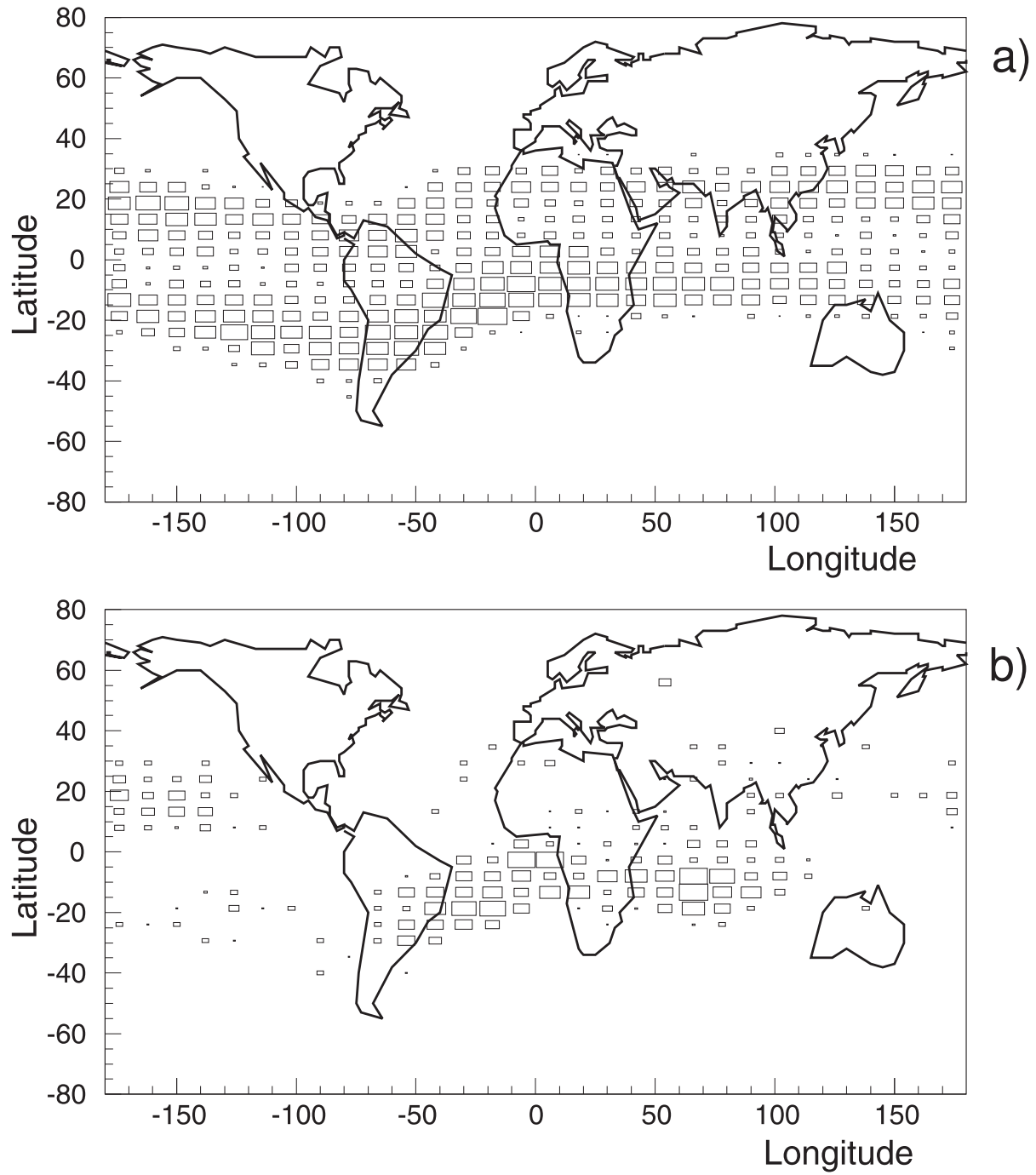


Figure 11: Maps of secondary protons end points for geomagnetic latitude  $|\theta_M| < 0.4$  rad. Figure (a) live time  $< 0.3s$  Figure (b) live time  $> 0.3s$

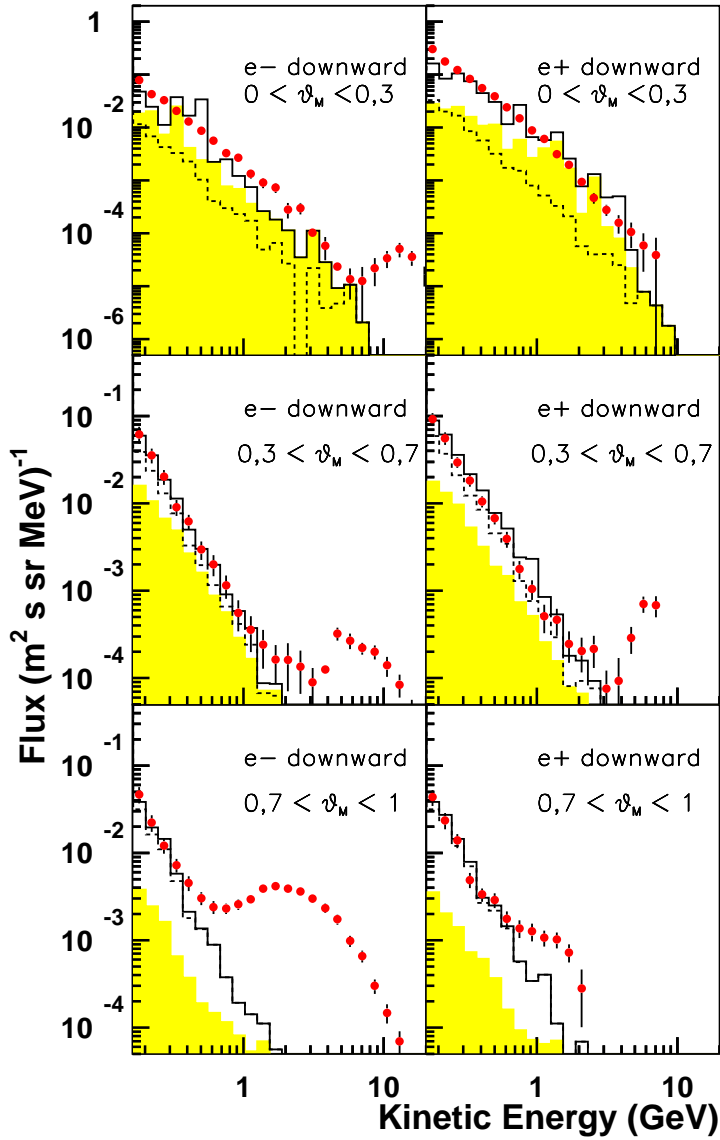


Figure 12: Downgoing positron and electron fluxes in two regions of geomagnetic latitude  $\theta_M$ , solid histogram (simulation) black points (AMS data); hatched histogram shows the positron and electron fluxes produced by primary protons with  $E_k > 30 \text{ GeV}$ ; the dashed line distributions are described in the text.

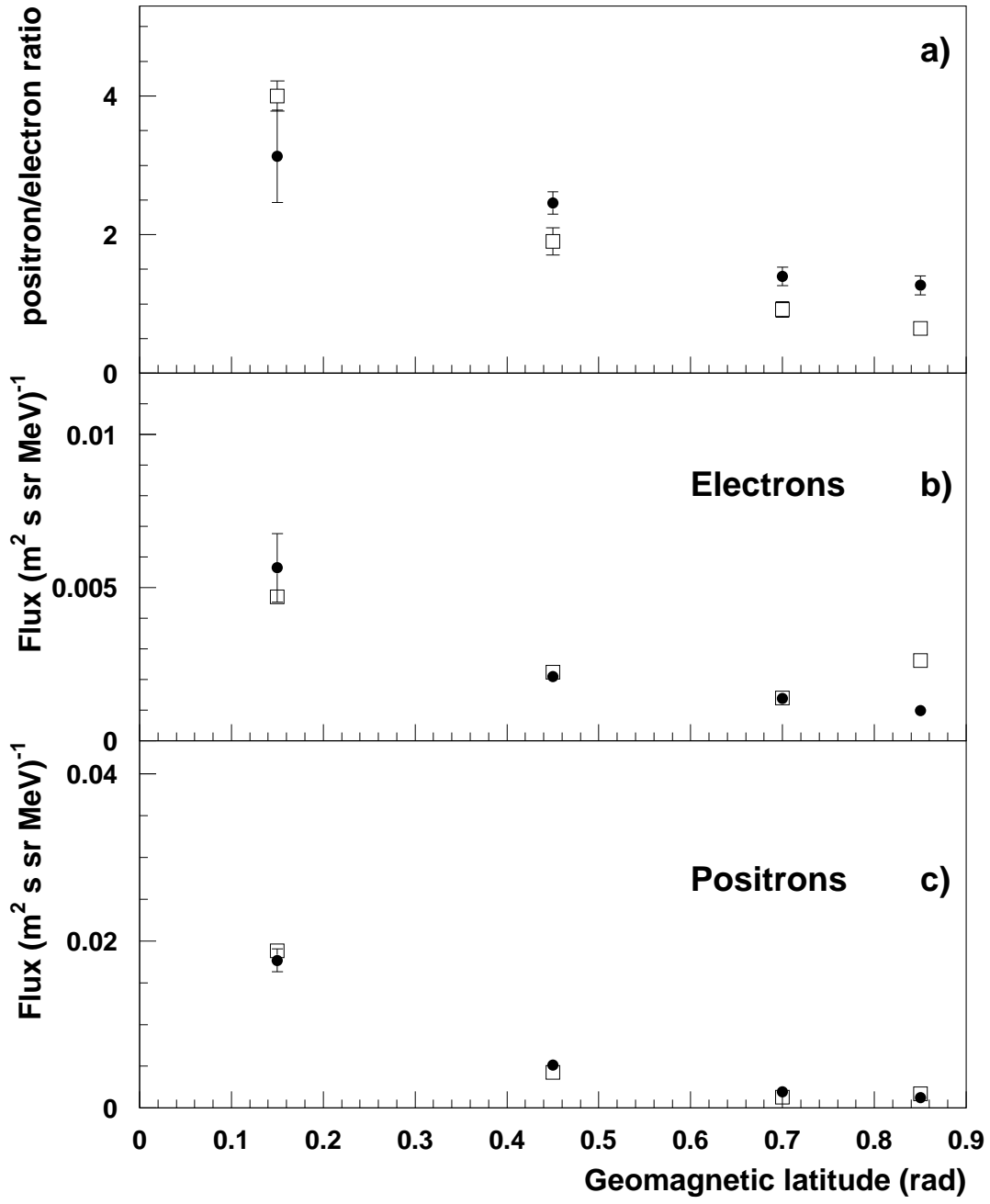


Figure 13: Electron (b) and positron (c) fluxes and their ratio (a) integrated in the kinetic energy range  $0.2 - 1.5 \text{ GeV}$ , as function of geomagnetic latitude. Open squares (AMS data), black points (simulation).